QUARTERLY JOURNAL OF THE ROYAL METEOROLOGICAL SOCIETY
Q. J. R. Meteorol. Soc. **134**: 1661–1671 (2008)
Published online in Wiley InterScience
(www.interscience.wiley.com) DOI: 10.1002/qj.327

Tropical-cyclone intensification and predictability in a minimal three-dimensional model

Seoleun Shin and Roger K. Smith*
Meteorological Institute, University of Munich, Munich, Germany

ABSTRACT: We investigate the amplification and predictability of tropical cyclones in the context of a minimal, three-dimensional numerical model. In the prototype problem for intensification, starting with a tropical storm strength vortex in a quiescent environment on an f-plane, the emergent flow in the inner region of the vortex becomes highly asymmetric and dominated by deep convective vortex structures, even though the problem as posed is essentially axisymmetric. The details of the intensification process, including the asymmetric structures that develop, are highly sensitive to small perturbations in the low-level moisture field at the initial time. This sensitivity is manifest in a significant spread in the intensity of vortices from an ensemble of calculations in which random moisture perturbations are added in the lowest model level. Similar experiments are carried out on a β-plane and in the case where there is an anticyclonic shear flow at upper levels. The former set shows no significant difference from the f-plane calculations in the evolution of intensity, but the latter set shows a significantly weaker vortex, contrary to a broadly held hypothesis that upper-level outflow channels are favourable to intensification.

KEY WORDS hurricane; tropical cyclone; typhoon; predictability; minimal model

Received 4 January 2008; Revised 2 September 2008; Accepted 3 September 2008

1. Introduction

In this paper we revisit the prototype problem for tropical-cyclone intensification, which considers the evolution of a prescribed, initially cloud-free, axisymmetric, baroclinic vortex over a warm ocean on an f-plane. This problem has been the subject of many numerical studies over the years and these can be classified into the following types:

- hydrostatic axisymmetric models with cumulus parametrization (e.g. Ooyama, 1969; Emanuel, 1989, 1995; Nguyen *et al.*, 2002);
- hydrostatic three-dimensional models with cumulus parametrization (e.g. Kurihara and Tuleya, 1974; Zhu *et al.*, 2001, hereafter ZSU; Zhu and Smith, 2002, 2003, hereafter ZS03; Zhu *et al.*, 2004);
- hydrostatic three-dimensional models with explicit microphysics (e.g. Wang 2001, 2002a, 2002b);
- non-hydrostatic axisymmetric cloud models (e.g. Willoughby *et al.*, 1984; Rotunno and Emanuel, 1987; Persing and Montgomery, 2003);
- non-hydrostatic three-dimensional cloud models (Montgomery *et al.*, 2006);
- non-hydrostatic three-dimensional mesoscale models (Nguyen *et al.*, 2008, hereafter NSM08).

A significant feature of all the three-dimensional calculations is the emergence of flow asymmetries, despite the symmetry in the formulation, except, of course, in the representation of a circular flow on a square grid or possibly the implementation of boundary conditions on a distant square boundary.

The related problem on a β-plane is the prototype problem for tropical-cyclone motion and has been a topic of much study also (e.g. Flatau *et al.*, 1994; Wang and Holland, 1996; Dengler and Reeder, 1997; Ritchie and Frank, 2007; NSM08). (There have been many more studies of this problem in a barotropic context, but our interest here is focused on baroclinic models with at least three vertical levels to represent the effects of deep convection.) However, in this case, flow asymmetries are expected to evolve from the lack of symmetry implied by β. Indeed, it is the wavenumber-one component of these asymmetries that leads to the well-known north-westward motion of the vortex.

The occurrence of asymmetries in f-plane calculations was the focus of a study by ZS03 in the context of a minimal three-layer model. At that time, we considered the asymmetries to be spurious and showed that their amplitude could be reduced by reformulating finite differences in the vertical on a Charney–Phillips (CP) grid instead of on a Lorenz grid as used by ZSU, Zhu and Smith (2002), and many others. The results suggested that the early development of asymmetries was exacerbated by a computational mode in temperature that is generated with the onset of convection. This computational mode does not occur with the CP grid. However, even with this grid, ZS03 found a weak wavenumber-four asymmetry in the temperature and velocity fields in the lower to

*Correspondence to: Roger K. Smith, Meteorological Institute, University of Munich, Theresienstr. 37, 80333 Munich, Germany.
E-mail: roger.smith@lmu.de

middle troposphere. It turns out that these asymmetries are associated with a significant asymmetry in the relative vorticity in this layer and we believe now that they are in some sense quasi-realistic features associated with an attempt of the model to resolve deep convection. This belief stems from the results of NSM2008, who used a higher-resolution multilayer model.

NSM08 showed that the flow asymmetries that develop are highly sensitive to the surface moisture distribution. When a random moisture perturbation is added in the boundary layer at the initial time, even with a magnitude that is below the accuracy with which moisture is normally measured, the pattern of evolution of the flow asymmetries is dramatically changed and no two such calculations are alike in detail. The same is true also of calculations on a β-plane, at least in the inner-core region of the vortex, within 100–200 km from the centre. Nevertheless, the large-scale β-gyre asymmetries remain coherent and are similar in each realization, so that they survive when one calculates the ensemble mean. The implication is that the inner-core asymmetries on the f- and β-planes result from the onset of model convection and that, like convection in the atmosphere, they have a degree of randomness, being highly sensitive to small-scale inhomogeneities in the low-level moisture distribution, which is a well-known characteristic of the real atmosphere (e.g. Weckwerth, 2000).

The recognition that the inner-core asymmetries are associated with convective processes motivated us to revisit the prototype intensification problem using the minimal three-dimensional hurricane model described by ZS03. The re-examination is important because the model is potentially useful for developing a basic understanding of tropical-cyclone dynamics and has been used to study the inner-core asymmetries when the model is coupled to a simple ocean model (Zhu *et al.*, 2004). The present version of the model has a higher horizontal resolution than that of ZS03 (10 km instead of 20 km) and has a simple explicit representation of moist processes, but no convective parametrization scheme. In particular, we investigate the structure and evolution of the flow asymmetries and the range of variability of the vortex intensity and structure when the boundary-layer moisture is slightly perturbed. This study complements that of NSM08.

The random nature of the inner-core asymmetries calls for a new methodology to assess differences between two particular flow configurations, because the results of a single deterministic calculation in each configuration may be unrepresentative of a model ensemble in that configuration. This means that one needs to compare the ensemble means of suitably perturbed ensembles of the two configurations. We illustrate this methodology in two examples of idealized flows.

The paper is structured as follows. In section 2 we give a brief description of the model. Then, in sections 3 and 4 we compare ensemble calculations of vortex evolution on an f-plane and on a β-plane, where the ensembles are generated by adding small moisture perturbations at low levels. In section 5 we apply the foregoing methodology to explore the effects of adding an anticyclonic shear flow to the upper model level. This problem is of interest because it has often been supposed that the presence of outflow channels in the upper troposphere is conducive to tropical-cyclone intensification (e.g. Sadler, 1976, 1978; Merrill, 1988). In the calculations shown here, the presence of the shear flow is found to be detrimental to intensification. The conclusions are given in section 6.

2. The model

The minimal hurricane model is that described in ZS03. It is fully three-dimensional and based on the hydrostatic primitive equations formulated in σ-coordinates (x, y, σ), where $\sigma = (p - p_{\text{top}})/(p_{\text{s}} - p_{\text{top}})$. Here, p is the pressure, p_{s} is the surface pressure and p_{top} is the pressure at the top of the domain. The vertical differencing is carried out on a CP grid shown in Figure 1. The model equations and the advantages of the CP grid are discussed by ZS03. The model is divided vertically into four layers of unequal depth in σ: the lowest layer has depth 0.1 and the three layers above have depths 0.3. Some of the calculations are carried out on an f-plane and some on a β-plane. Newtonian cooling is used to represent the effect of radiative cooling. Simply, the moist static energy is relaxed to its environmental value on a prescribed time-scale, τ. The turbulent flux of momentum to the sea surface and the fluxes of sensible heat and water vapour from the surface are represented by bulk aerodynamic formulae. The surface drag coefficient, C_{D}, is calculated from the formula used by Shapiro (1992):

$$C_{\text{D}} = (1.024 + 0.05366 R_{\text{F}} |\mathbf{u}_{\text{b}}|) \times 10^{-3}. \qquad (1)$$

Here, $R_{\text{F}} = 0.8$ is used to reduce the boundary layer wind, $\mathbf{u}_{\text{b}}$, to the 10-m level. The surface exchange coefficients for moisture and heat are assumed to be equal to each other and to C_{D}.

Moist processes are represented in this version of the model by the simplest explicit scheme in which condensation occurs when the air becomes supersaturated at a grid point. At such points, the excess water is assumed to precipitate out and the latent heat of the

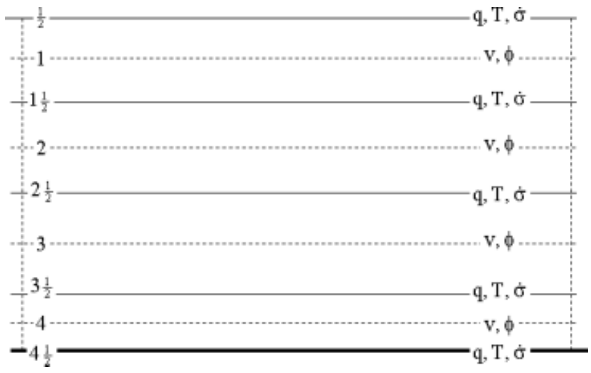

Figure 1. The CP vertical grid used in the model.

DOI: 10.1002/qj

Table I. The numerical experiments.

Number	Name	Description
A0	Control	Control experiment on an f-plane, quiescent environment
A1–A10	f-plane ensemble	Ten ensemble members (see text for details)
B1–B10	f-plane ensemble	Same as A0–A10, except with a smaller ($\times 1/4$) moisture perturbation
C0–C10	β-plane ensemble	Same as A0–A10, except on a β plane
D0–D10	f-plane ensemble	Same as A0–A10, except with an anticyclonic upper-level shear flow

condensed water goes to increase the air temperature. The scheme, which is described in detail by ZSU, involves an iterative procedure. There is no parametrization of deep convection as in the original model.

The initial vortex is axisymmetric and baroclinic. The tangential wind profile is that used by Smith *et al.* (1990), but with different parameters: the maximum tangential wind speed is 15 m s^{-1} at level 4 at a radius of 120 km and its magnitude reduces to zero at level 1. The initial mass and geopotential fields are obtained by solving the inverse balance equation in the same way as Kurihara and Bender (1980). The far-field temperature, geopotential height and humidity structure are based on the mean West Indies sounding (Jordan, 1957). The horizontal grid spacing of the model is 10 km and the integration time step is 3 s. The ocean surface temperature is 26.3°C. The experiments are performed on an f-plane at 20°N. As in ZS03, the value of τ is taken to be ten days following the suggestion of Mapes and Zuidema (1996). The vortex centre is obtained by calculating a centre of weighted relative vorticity evaluated over the area 400 × 400 km^2 centred on the location of maximum relative vorticity.

Four main sets of calculations are carried out as summarized in Table I. The first set, the control set, consists of a standard calculation (A0) and ten additional ones (A1–A10) in which the moisture fields throughout the innermost domain are randomly perturbed at the surface (i.e. at level 4 1/2 and level 3 1/2). In the latter, the magnitude of the mixing ratio perturbation lies in the range of (-0.5 g kg^{-1}, 0.5 g kg^{-1}). The integration time is 120 h.

3. Experiments on an f-plane

We describe first the development of the initial axisymmetric vortex in the f-plane experiments (A0–A10 in Table I). Figure 2 shows a time series of the maximum, azimuthally averaged, total wind speed near the top of the boundary layer ($\sigma = 0.95$), during a 120 h integration in these experiments. The average is performed about the centroid of the vertical component of relative vorticity. We call this average wind speed $vT_{\max}$ and use it to characterize the intensity of the vortex at any given time. As in many previous calculations relating to the present thought experiment, the vortex evolution begins with a gestation period during which it slowly decays as a result of surface friction. However, the boundary layer progressively moistens because of evaporation from the underlying sea surface. The imposition of friction from the initial instant leads to a breakdown of gradient-wind balance in a shallow boundary layer and thereby to a net inward force (e.g. Smith, 1968). This force drives inflow in the boundary layer, which, through continuity, is accompanied by outflow above the layer. The early decay of the vortex is a result of this outflow, combined with the conservation of absolute angular momentum as air parcels move outwards. The moist inflowing air cools as it rises out of the boundary layer and expands. Eventually, condensation occurs in some grid columns near the radius of maximum tangential wind speed, r_{m}. Then, as shown below, 'model' convective clouds develop rapidly and soon afterwards the vortex rapidly intensifies.

3.1. Vortex evolution in the control experiment

The changes in vortex structure during the later period of rapid intensification, between 42 and 48 h, are exemplified by those in the control calculation A0. In this experiment, there is no moisture perturbation in the boundary layer. The evolution is highlighted by the fields of vertical σ-velocity ($\dot{\sigma}$) at $\sigma = 0.9$ (Figure 3), the vertical component of relative vorticity at $\sigma = 0.95$ (Figure 4) and the total wind speed at this level (Figure 5). At 42 h,

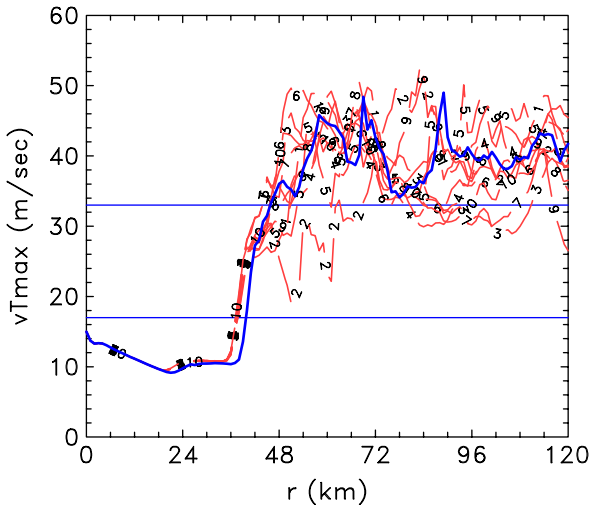

Figure 2. Time series of the azimuthally averaged total wind speed maximum at the σ-level 0.95 in experiments A0–A10. The thick solid curve denotes the control run A0 and the thin curves the ten ensembles, numbered 1–10 (see section 3.2). This figure is available in colour online at www.interscience.wiley.com/journal/qj

DOI: 10.1002/qj

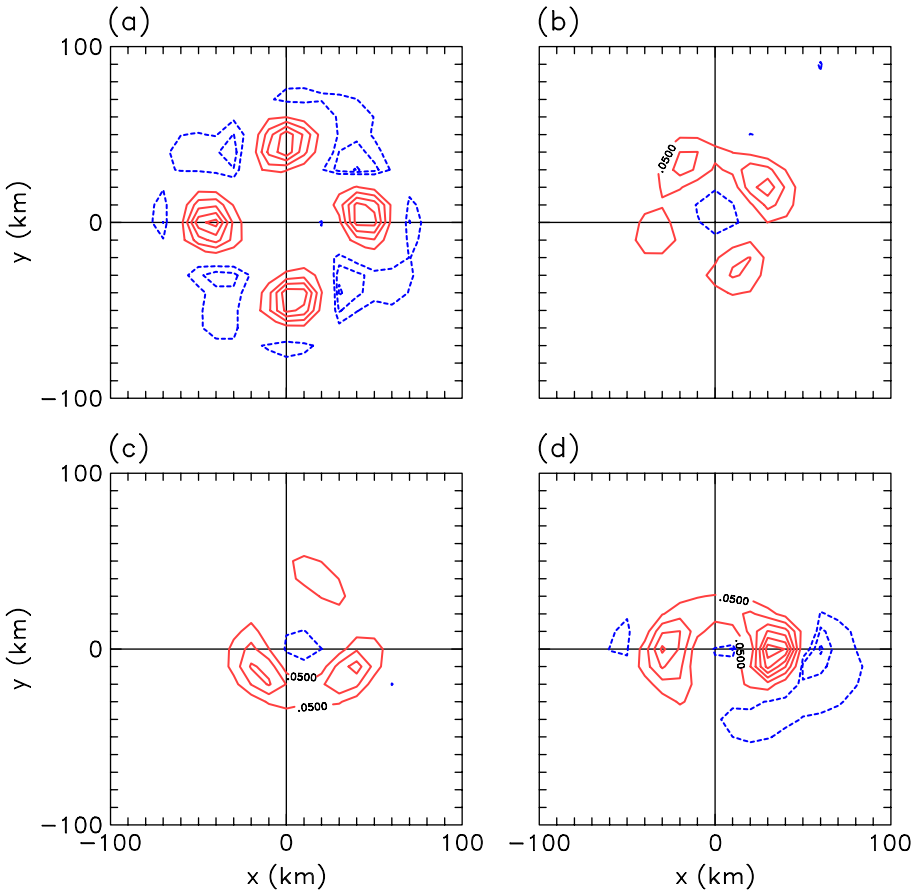

Figure 3. Vertical σ-velocity fields ($\dot{\sigma}$) for the control experiment A0 at (a) 42 h, (b) 44 h, (c) 46 h and (d) 48 h. The contour interval is 1×10^{-5} s^{-1} for positive values (solid curves) and 5×10^{-5} s^{-1} for negative values (dashed curves). Negative values of $\dot{\sigma}$ indicating upward motion are plotted with solid contours and positive values are dashed. The zero contour is not plotted. This figure is available in colour online at www.interscience.wiley.com/journal/qj

there are four 'convective cells' located at the corners of a square at a radius of about 50 km from the vortex centre (Figure 3a). The pattern of evolution of the relative vorticity (Figure 4) and the total wind field (Figure 5) are similar to that of the vertical velocity. Moreover, comparing Figures 3 and 4, it is seen that the updrafts possess significant local rotation. The rotation is locally enhanced as relative vorticity is stretched and amplified. As time proceeds, the rotating updrafts circle around the vortex axis cyclonically and spiral inwards so that they interact and rapidly merge (Figure 4). Indeed, in just a six-hour period their initial wavenumber-four pattern has practically disappeared. Thus, although the calculation begins with an axisymmetric vortex in a quiescent environment on an f-plane, the vortex intensification process is intrinsically non-axisymmetric. The foregoing evolution is similar to that in the high-resolution cloud-resolving vortex simulations described by Hendricks *et al.* (2004), Montgomery *et al.* (2006) and NSM08. These simulations, which used horizontal grid spacings of between 5 and 1.67 km, showed that intense vorticity anomalies are produced by buoyant cores growing in the rotation-rich environment of an incipient vortex and that these convective cores subsequently undergo merger and axisymmetrization. Following these authors, we refer to the rotating updrafts as 'vortical hot towers' (VHTs). Of course, with a horizontal grid spacing of 10 km, the VHTs in our model are not adequately resolved and they are hydrostatic.

After a slight decline in intensity between 53 and 56 h, the vortex begins again to intensify to reach what might be described as a quasi-steady state, the period after about 60 h (Figure 2). The mean intensity between 60 and 120 h is 40.3 m s^{-1}, but there are significant fluctuations during this period, the standard deviation being 3.2 m s^{-1}. As in the calculations of NSM08, it is found that these fluctuations are associated with major convective outbreaks and axisymmetrization of the vortex is never complete. The question is, how significant are the individual fluctuations in intensity? This question is addressed in the next section.

3.2. Vortex evolution in the ensemble experiments

Figure 2 shows also the evolution of intensity in the ensemble calculations A1–A10, in which the low-level moisture field is randomly perturbed. It is notable that the onset of the rapid intensification occurs earlier than in the control calculation A0 in all these calculations. While this result may be surprising at first sight, the reason is that

DOI: 10.1002/qj

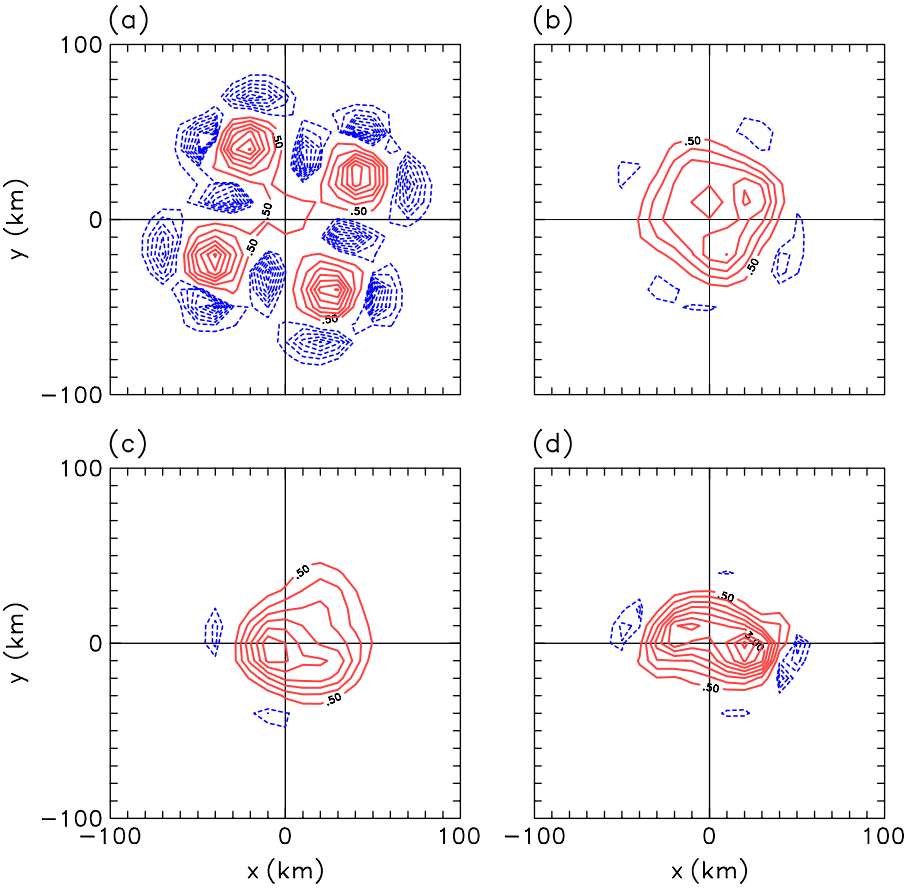

Figure 4. The vertical component of the relative vorticity fields of the control experiment A0 at (a) 42 h, (b) 44 h, (c) 46 h and (d) 48 h. The contour interval is 5×10^{-4} s^{-1} for positive values (solid curves) and 5×10^{-5} s^{-1} for negative values (dashed curves). The zero contour is not plotted. This figure is available in colour online at www.interscience.wiley.com/journal/qj

although the moisture perturbation in a particular ensemble member is spatially random, there are always some positive perturbations that initiate deep convection earlier. In fact, grid-scale saturation at $\sigma = 0.9$ occurs at about 18 h in all the ensembles, which is about 2 h earlier than in the control run and this leads to a correspondingly earlier development of the VHTs. We see this in the pattern of relative vorticity in the ensemble members A1–A3 at 38 h (Figure 6), fields which are similar to that in the control experiment at 40 h. While the differences between ensemble members at this time are slight, the solutions rapidly diverge, as shown in the corresponding vorticity fields at 45 h in A0 and 43 h in A1–A3 shown in Figure 7. These differences provide an explanation for the differences in intensity between the control experiment and the ensembles evident in Figure 2 and provide an answer to the question raised in section 3.1. It is manifestly clear that the differences in intensity are not significant, rather they are random features associated with small random perturbations of low-level moisture.

As one measure of the variability in the ensemble calculations, we calculated the maximum total wind speed attained over the 120 h integration period and the time at which this maximum was reached. The average maximum (with the control calculation included) was 48.9 m s^{-1}, with a standard deviation of 2.3 m s^{-1}. The time at which this maximum occurs shows considerable variability also, the average time being at 76 h and the standard deviation 15 h. We carried out a second set of ensemble calculations (B1–B10) with the amplitude of the moisture perturbation reduced by a factor of 4 to enable the calculations to be better compared with those of NSM08, who used grid cells of one-quarter the area of those here. In this case, the average maximum wind speed increased slightly to 52.5 m s^{-1} with a standard deviation of 4.2 m s^{-1}. The time at which the maxima occur showed a similar variability, the average being again at 76 h, but the standard deviation 17 h is marginally larger.

Figure 8 compares the time series of the ensemble mean of the azimuthally averaged total wind speed maximum in the boundary layer (i.e. at $\sigma = 0.95$) in the two sets of ensemble calculations A0–A10 and B1–B10. Perhaps surprisingly, the variability between ensemble members in B1–B10 is larger than in A0–A10, as indicated by the standard deviation time series, shown also in Figure 8. We are not yet able to explain this result, but infer therefrom that it is not the horizontal resolution that leads to the greater variability in these minimal model calculations compared with NSM08. Another possibility is that it is the coarser vertical resolution that is responsible, a possibility that we plan to investigate in due course.

DOI: 10.1002/qj

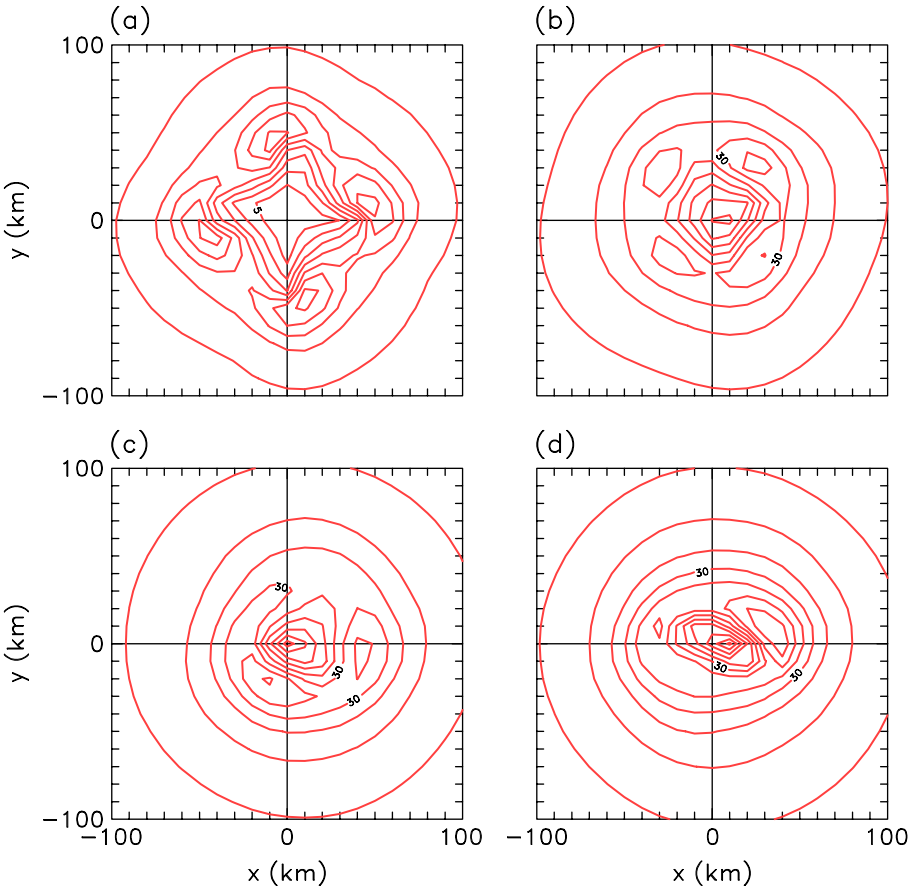

Figure 5. Total wind fields at σ-level 0.95 in the control experiment A0 at (a) 42 h, (b) 44 h, (c) 46 h and (d) 48 h. The contour interval is 5 m s^{-1}. This figure is available in colour online at www.interscience.wiley.com/journal/qj

4. Experiments on a β-plane

At this stage, it is of interest to examine how the evolution of the flow asymmetries is affected by the presence of a β-effect, the relevant question being, to what extent does the azimuthal wavenumber-one asymmetry imposed by β impose a stamp on the asymmetries that develop? For this reason, we repeated the ensemble f-plane experiments described in section 3.1 for the β-plane. These experiments are designated C0–C10 in Table I. A time series of the ensemble average of the azimuthally averaged total wind speed maxima in the boundary layer for experiments A0–A10 is compared with that for the experiments C0–C10 in Figure 9. There is virtually no difference between the two curves until about 40 h and there is no significant difference after about 63 h, when the two curves lie largely within one standard deviation of the variability in each ensemble (indicated by the vertical lines in Figure 9). In the intervening period, which marks the second part of the period of rapid intensification, the intensity in the ensemble mean intensity on the f-plane is a little larger, by up to 5 m s^{-1}, compared with the mean intensity on the β-plane. Even then, the deviation hardly exceeds one standard deviation of the variability in each ensemble, except in the last 12 h of the calculations. We conclude that there is no significant difference between the intensity in the f- and β-plane calculations. Note, however, that it is necessary to carry out ensemble calculations to demonstrate this lack of a significant difference; had we chosen to compare two ensemble members, one from each set of calculations, we may have arrived at a different conclusion. This possibility is indicated by the substantial variation in intensity between individual members in the case of the f-plane calculations shown in Figure 2, a result that is true also of those on the β-plane.

The inner-core asymmetries in the β-plane calculations are again dominated by random 'model' convective bursts as in the f-plane experiments and do not show up as a coherent asymmetry in the ensemble mean. This feature is exemplified by the azimuthal wavenumber-one component of relative vorticity for the f-plane shown in Figures 6 and 7. Nevertheless, a coherent large-scale asymmetry is apparent in the ensemble average fields (Figure 10) and corresponds with the associated β-gyres familiar in barotropic calculations (e.g. Fiorino and Elsberry, 1989; Smith and Ulrich, 1990, 1993; Smith *et al.*, 1990). Note that the strength of these asymmetries increases with time during the 12 h period from 48 to 60 h and their scale increases, as would be expected from barotropic theory (Smith and Ulrich, 1993). A similar result was obtained in the high-resolution calculations of NSM08.

Our conclusions here differ significantly from those of a very recent paper by Ritchie and Frank (2007).

DOI: 10.1002/qj

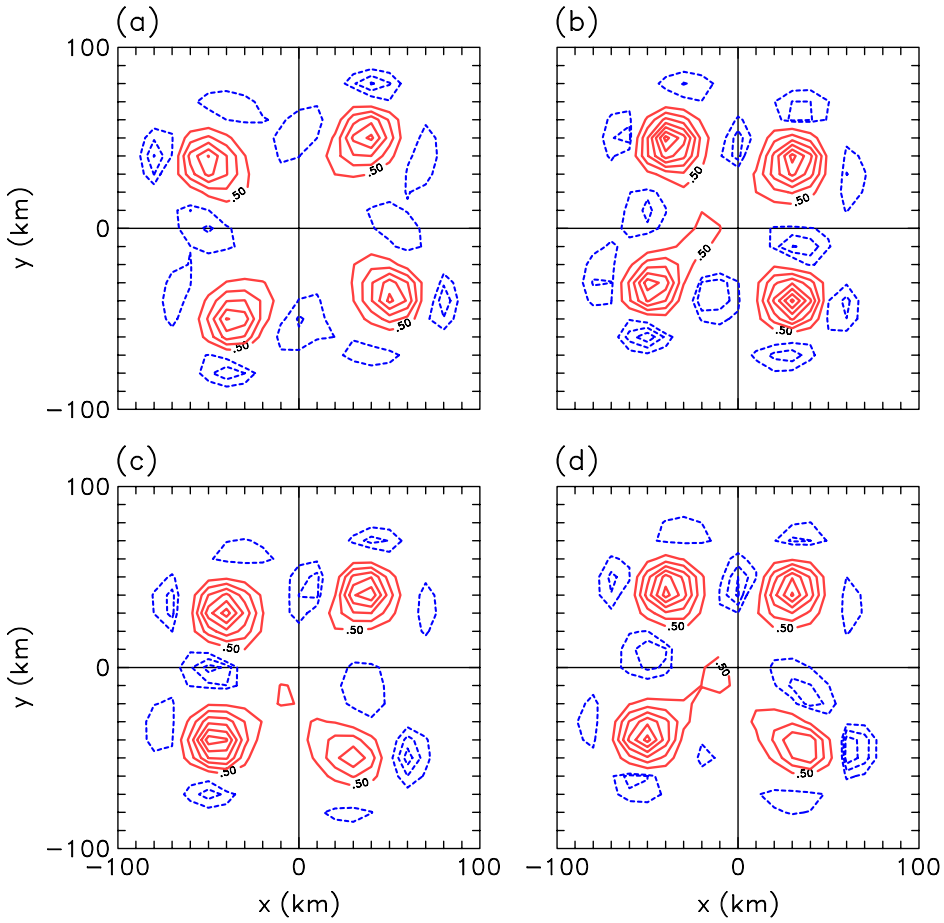

Figure 6. Vertical component of the relative vorticity in (a) the control experiment A0 at 40 h, and in three of the ensemble experiments (b) A1, (c) A2 and (d) A3 at 38 h. The contour interval is 5×10^{-4} s^{-1} for positive values (solid curves) and 1×10^{-4} s^{-1} for negative values (dashed curves). The zero contour is not plotted. This figure is available in colour online at www.interscience.wiley.com/journal/qj

They compared two deterministic experiments of a similar type to ours using a version of the Pennsylvania State University–National Center for Atmospheric Research fifth-generation Mesoscale Model (MM5) with 5 km horizontal resolution. They found that the vortex on the β-plane 'quickly develops a persistent wavenumber-one asymmetry in its inner core'. Based on our ensemble experiments and those of NSM08, we question the validity of this conclusion. Unfortunately, it is not possible to compare the details of vortex evolution in our control experiments with theirs, as they show only coarse-grain, horizontal fields of potential vorticity and only at the mature stage of vortex development. Nevertheless, we note that they found little difference in the intensity between their f- and β-plane experiments, consistent with our results.

5. Experiments with an upper-level anticyclonic shear flow on an f-plane

It is commonly believed that a favourable condition for tropical-cyclone intensification is the existence of so-called outflow channels in the upper troposphere that provide a means of assisting the removal of air that rises in the eyewall. As far as we are aware, this idea was first put forward by Sadler (1976) and it seems to have gained much credence amongst forecasters, some of whom see it as a mechanism for 'sucking' air upwards in the storm and thereby enhancing the secondary circulation as well as the low-level convergence. Merrill (1988) suggested that the outflow is enhanced by the approach of a jet stream associated with an upper-level trough, thereby enhancing the secondary circulation of the jet. If the upward branch of the secondary circulation is close enough to the cyclone, it might invigorate the inner-core convection.

Shi *et al.*, (1990) carried out a series of idealized numerical experiments with a view to testing these ideas. The idea was to examine the response of the model cyclone to an acceleration of the outflow brought about by artificially nudging parts of the outflow to a specified wind distribution. When the nudging was performed within 5° latitude of the vortex, the storm did strengthen. However, when it was performed outside this radius, convection was initiated far from the storm axis and the storm weakened.

An alternative perspective on these issues is to recognize that deep convection is a response to conditional instability and that the outflow channels are generated by the inner-core convection, itself. This idea is supported by the scale analysis of tropical motions by Charney

DOI: 10.1002/qj

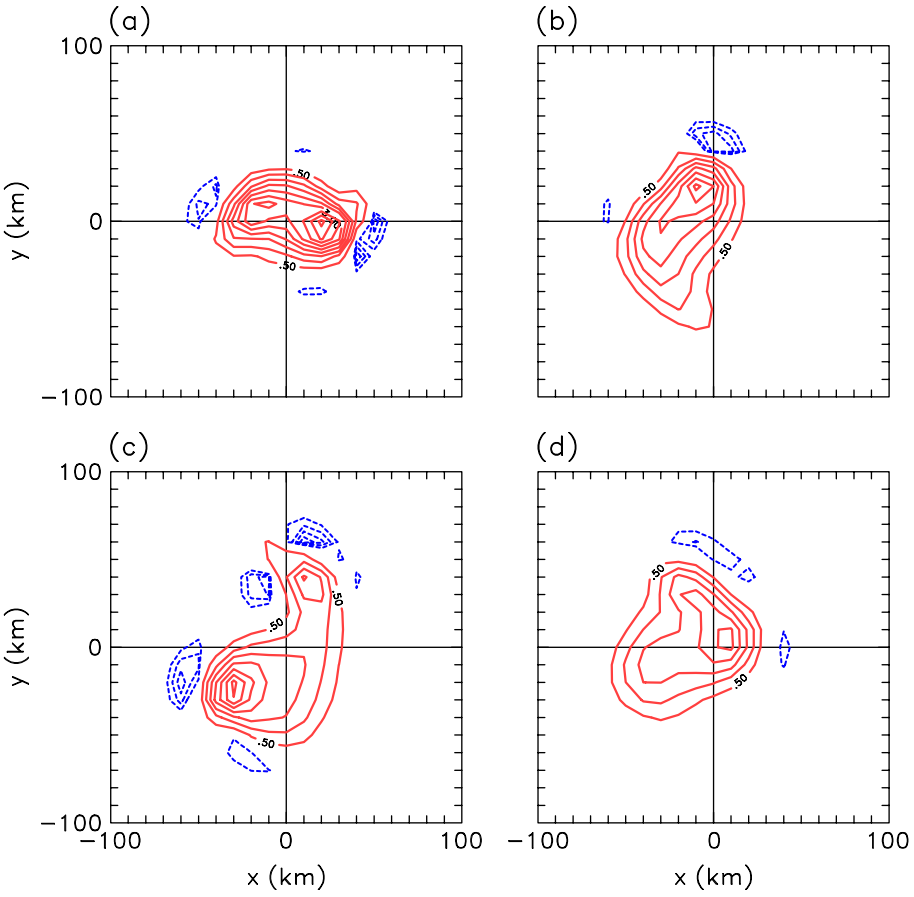

Figure 7. Vertical component of the relative vorticity in (a) the control experiment A0 at 45 h, and in three of the ensemble experiments at 43 h: (b) A1, (c) A2 and (d) A3. The contour interval is 5×10^{-4} s^{-1} for positive values (solid curves) and 5×10^{-5} s^{-1} for negative values (dashed curves). The zero contour is not plotted. This figure is available in colour online at www.interscience.wiley.com/journal/qj

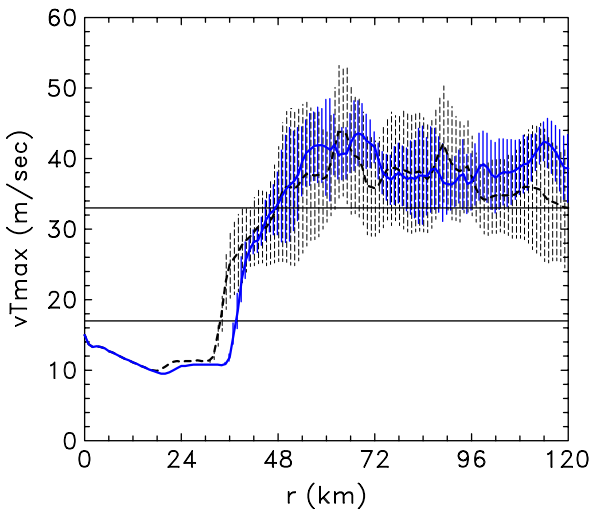

Figure 8. Comparison of time series of the ensemble mean of the azimuthally averaged total wind speed maximum at the σ-level 0.95 in the ensemble calculations A0–A10 (solid line) and B0–B10 (dashed line), referred to in section 3.2. The thin vertical lines indicate the standard deviation (solid lines for A0–A10 and dashed lines for A0 and B1–B10). This figure is available in colour online at www.interscience.wiley.com/journal/qj

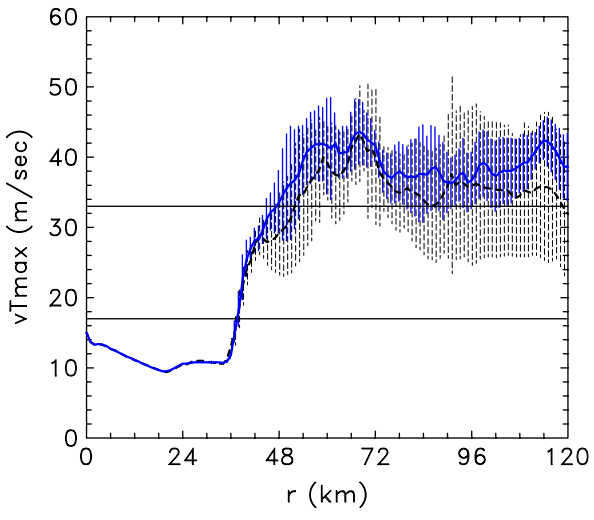

Figure 9. Comparison of time series of the ensemble mean of the azimuthally averaged total wind speed maximum at the σ-level 0.95 in the ensemble calculations A0–A10 (solid lines) and those on the β-plane, C0–C10 (dashed lines). The thin vertical lines indicate the standard deviation (solid lines for A0–A10 and dashed lines for C0–C10). This figure is available in colour online at www.interscience.wiley.com/journal/qj

DOI: 10.1002/qj

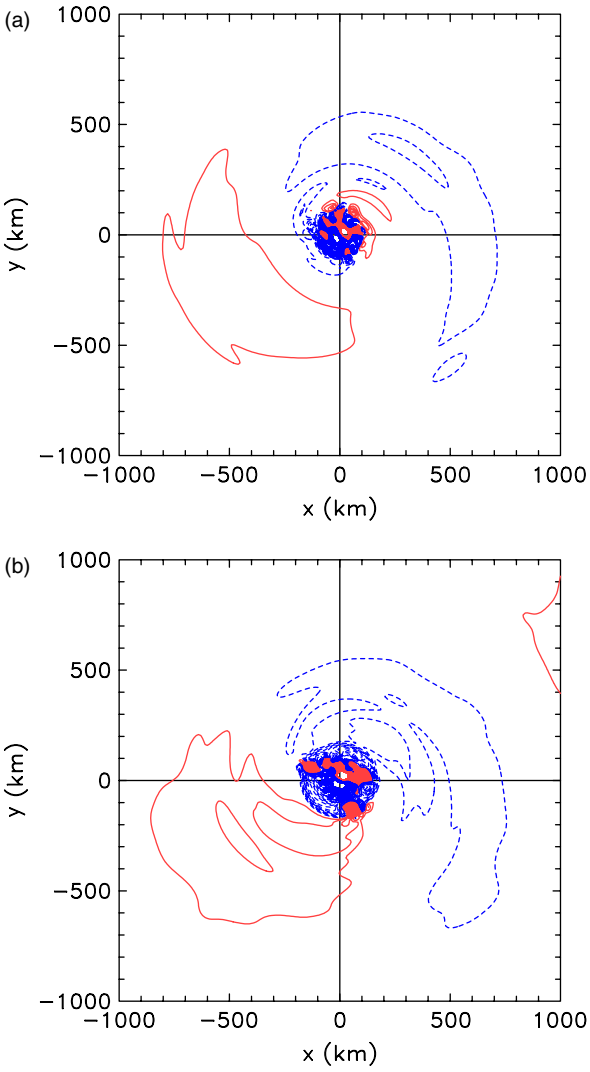

Figure 10. Ensemble average of the vertical component of relative vorticity at $\sigma = 0.95$ in the β-plane calculations C0–C10 at (a) 48 h and (b) 60 h. The contour interval is 2×10^{-6} s^{-1} for both positive values (solid curves) and negative values (dashed curves). The zero contour is not plotted. This figure is available in colour online at www.interscience.wiley.com/journal/qj

(1963), which shows that in the absence of diabatic forcing, synoptic-scale flows in the Tropics are effectively horizontally non-divergent, a finding that would apply specifically to the flow surrounding tropical cyclones. To our knowledge, this perspective has not been examined using numerical models and such is the motivation of this section. Our plan is to use the minimal model and the ensemble methodology described above to test the hypothesis that the presence of outflow channels is favourable to intensification in our model. To do this, we carried out an additional set of experiments identical to A0–A10, except that an upper-level anticyclonic shear flow was imposed at the model-level $\sigma = 0.15$, where there is initially no motion in the previous experiments. We refer to these experiments as D1–D10. The meridional wind, U, is given by

$$U(y) = 10 \tanh\left(\frac{y}{400}\right) \text{ m s}^{-1},$$

where y is the meridional coordinate in km. Then the meridional wind speed is approximately 10 m s^{-1} at $y =$ 1000 km. The balanced temperature field of this mean flow together with the initial vortex were obtained in the same way as in the other calculations (see section 2). We now ask the question, does the presence of the shear flow enhance the intensification rate of the model tropical cyclone?

Figure 11 compares a time series of the ensemble average of the azimuthally averaged total wind speed maximum in the boundary layer in the experiments D0–D10 with that for a quiescent environment, A0–A10. The evolution of mean intensity is similar in both sets of experiments during the gestation period, the first 36 h. However, the intensification begins slightly earlier in the case of a quiescent environment and the subsequent intensification is more rapid. In fact, during the rapid intensification phase, between 36 and 72 h, the mean intensity in the cases with 'favourable' outflow channels is less than that in the case of the quiescent environment by up to 20 m s^{-1}. During the mature stage, after about 72 h, the difference is only about 5 m s^{-1}, but it increases again after 96 h. The spread in intensity (indicated by the vertical bars in Figure 11) is generally larger in the shear-experiment set than in the f-plane set after about 60 h. The reason for the differences in the ensemble-mean intensity can be traced to the fact that the upper-level shear flow is associated through thermal wind balance with a warm anomaly over the cyclone core (see Figure 12). This warm anomaly reduces the degree of convective instability created by surface evaporation and leads to a weaker secondary circulation within the cyclone. In other words, these simple idealized calculations, at least, do not support the hypothesis that outflow channels are favourable to intensification.

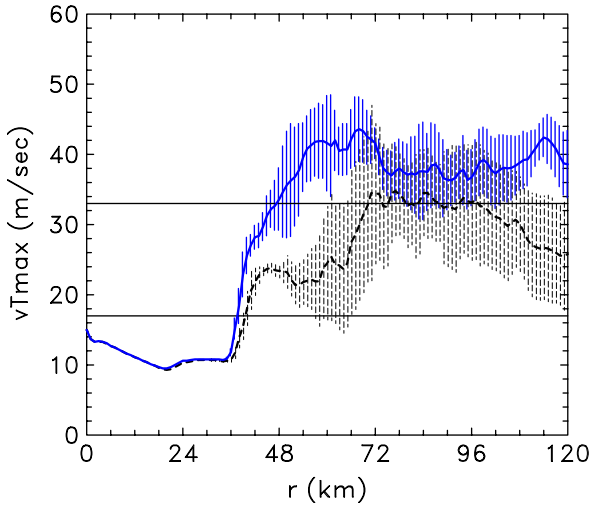

Figure 11. Ensemble average time series of the azimuthally averaged total wind speed maximum in the f-plane experiments A0–A10 (thick curve) and shear-flow experiments D0–D10 (thin curve). The thin vertical lines indicate the standard deviation (solid lines for A0–A10 and dashed lines for D0–D10). This figure is available in colour online at www.interscience.wiley.com/journal/qj

DOI: 10.1002/qj

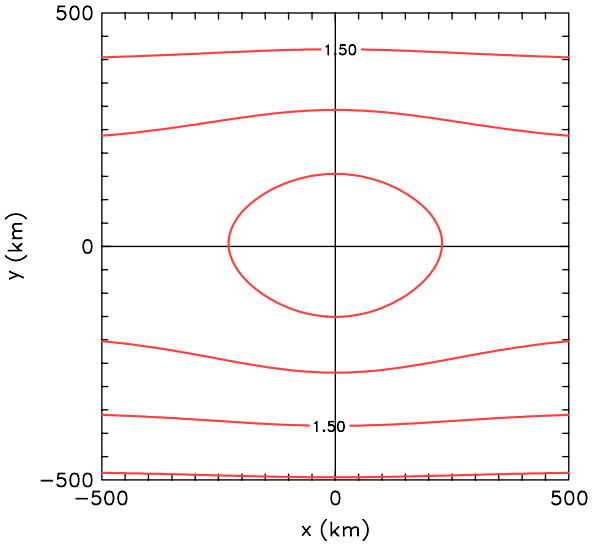

Figure 12. Upper-level (level 1) temperature anomaly relative to the far-field temperature at the same level and at the initial time in the shear-flow experiments. The contour interval is 0.5 K. This figure is available in colour online at www.interscience.wiley.com/journal/qj

6. Conclusions

We have shown that the predictability of hurricane intensity using the minimal hurricane model is limited by the sensitivity of the solutions to small, but random perturbations to the low-level moisture field. The results are in line with those of NSM08, who used a more complex, although also considerably idealized non-hydrostatic model.

The sensitivity to random moisture perturbations is larger with the 10 km grid size used here compared with the 5 km resolution grid size used by NSM08. This sensitivity is quantified in terms of the standard deviation of the intensity of a set of ensemble calculations. We ruled out that this increased sensitivity is because the implied horizontal scale of moisture fluctuations is larger than in NSM2008. The likelihood is that it is associated with the much coarser vertical resolution in the minimal model.

Together with that of NSM08, our study represents a new approach to understanding hurricane dynamics using models. It adopts the view that a single deterministic calculation may have features that are not significant when one takes into account the variability associated with the uncertainty in the low-level moisture distribution. In this view, only features that survive in an ensemble mean can be regarded as robust.

We have shown two examples of this approach: one in a comparison of vortex evolution on an f-plane with that on a β-plane and the other examining the role of apparently favourable outflow channels. In the latter case, the presence of outflow channels was found to be detrimental to intensification because the warm upper-level thermal anomaly between them has a stabilizing effect on deep convection in the intensifying vortex.

Acknowledgements

We are most grateful to Hongyan Zhu for kindly making her model available for this study, and to Michael Montgomery and two anonymous reviewers for their helpful comments on an earlier version of the manuscript. The first author is indebted to the Deutsche Akademischer Austauschdienst (DAAD) for providing a stipendium to support this study.

References

Charney JG. 1963. A note on the large-scale motions in the tropics. *J. Atmos. Sci.* **20**: 607–609.
Dengler K, Reeder MJ. 1997. The effects of convection and baroclinicity on the motion of tropical-cyclone-like vortices. *Q. J. R. Meteorol. Soc.* **123**: 699–727.
Emanuel KA. 1989. The finite amplitude nature of tropical cyclogenesis. *J. Atmos. Sci.* **46**: 3431–3456.
Emanuel KA. 1995. Sensitivity of tropical cyclones to surface exchange coefficients and a revised steady-state model incorporating eye dynamics. *J. Atmos. Sci.* **52**: 3969–3976.
Fiorino M, Elsberry R. 1989. Some aspects of vortex structure related to tropical cyclone motion. *J. Atmos. Sci.* **46**: 975–990.
Flatau M, Schubert WH, Stevens DE. 1994. The role of baroclinic processes in tropical cyclone motion. Part I: The influence of vertical tilt. *J. Atmos. Sci.* **51**: 2589–2601.
Frank WM, Ritchie EA. 1999. Effects of environmental flow upon tropical cyclone structure. *Mon. Weather Rev.* **127**: 2044–2061.
Hendricks EA, Montgomery MT, Davis CA. 2004. On the role of 'vortical' hot towers in formation of tropical cyclone Diana (1984). *J. Atmos. Sci.* **61**: 1209–1232.
Jordan CL. 1957. Mean soundings for the West Indies area. *J. Meteorol.* **15**: 91–97.
Kurihara Y, Bender MA. 1980. Use of a movable nested-mesh model for tracking a small vortex. *Mon. Weather Rev.* **108**: 1792–1809.
Kurihara Y, Tuleya RE. 1974. Structure of a tropical cyclone developed in a three-dimensional numerical simulation model. *J. Atmos. Sci.* **31**: 893–919.
Mapes BE, Zuidema P. 1996. Radiative-dynamical consequences of dry tongues in the tropical troposphere. *J. Atmos. Sci.* **53**: 620–638.
Merrill RT. 1988. Environmental influences on hurricane intensification. *J. Atmos. Sci.* **45**: 1678–1687.
Montgomery MT, Nicholls ME, Cram TA, Saunders AB. 2006. A vortical hot tower route to tropical cyclogenesis. *J. Atmos. Sci.* **63**: 355–386.
Nguyen CM, Smith RK, Zhu H, Ulrich W. 2002. A minimal axisymmetric hurricane model. *Q. J. R. Meteorol. Soc.* **128**: 2641–2661.
Nguyen SV, Smith RK, Montgomery MT. 2008. Tropical-cyclone intensification and predictability in three dimensions. *Q. J. R. Meteorol. Soc.* **134**: 563–582 (NSM08).
Ooyama KV. 1969. Numerical simulation of the life cycle of tropical cyclones. *J. Atmos. Sci.* **26**: 3–40.
Peng MS, Jeng BF, Williams RT. 1999 A numerical study on tropical cyclone intensification. Part I: Beta effect and mean flow effect. *J. Atmos. Sci.* **56**: 1404–1423.
Persing J, Montgomery MT. 2003. Hurricane superintensity. *J. Atmos. Sci.* **60**: 2349–2371.
Ritchie EA, Frank WM. 2007. Interactions between simulated tropical cyclones and an environment with a variable Coriolis parameter. *Mon. Weather Rev.* **135**: 1889–1905.
Rotunno R, Emanuel KA. 1987. An air–sea interaction theory for tropical cyclones. Part II: Evolutionary study using a non-hydrostatic axisymmetric numerical model. *J. Atmos. Sci.* **44**: 542–561.
Sadler JC. 1976. A role of the tropical upper tropospheric trough in early season typhoon development. *Mon. Weather Rev.* **104**: 1266–1278.
Sadler JC. 1978. Mid-season typhoon development and intensity changes and the tropical upper tropospheric trough. *Mon. Weather Rev.* **106**: 1137–1152.
Shapiro LJ. 1992. Hurricane vortex motion and evolution in a three-layer model. *J. Atmos. Sci.* **49**: 140–153.
Shi JJ, Chang SW, Raman S. 1990. A numerical study of the outflow of tropical cyclones. *Mon. Weather Rev.* **118**: 2042–2055.

Smith RK. 1968. The surface boundary layer of a hurricane. *Tellus* **20**: 473–483.
Smith RK, Ulrich W. 1990. An analytical theory of tropical cyclone motion using a barotropic model. *J. Atmos. Sci.* **47**: 1973–1986.
Smith RK, Ulrich W. 1993. Vortex motion in relation to the absolute vorticity gradient of the vortex environment. *Q. J. R. Meteorol. Soc.* **119**: 207–215.
Smith RK, Ulrich W, Dietachmayer G. 1990. A numerical study of tropical cyclone motion using a barotropic model. Part I: The role of vortex asymmetries. *Q. J. R. Meteorol. Soc.* **116**: 337–362.
Wang Y. 2001. An explicit simulation of tropical cyclones with a triply nested movable mesh primitive equation model: TCM3. Part I: Model description and control experiment. *Mon. Weather Rev.* **129**: 1370–1394.
Wang Y. 2002a. Vortex Rossby waves in a numerical simulated tropical cyclone. Part I: Overall structure, potential vorticity, and kinetic energy budgets. *J. Atmos. Sci.* **59**: 1213–1238.
Wang Y. 2002b.. Vortex Rossby waves in a numerical simulated tropical cyclone. Part II: The role in tropical cyclone structure and intensity changes. *J. Atmos. Sci.* **59**: 1239–1262.
Wang Y, Holland GJ. 1996. The beta drift of baroclinic vortices. Part II: Diabatic vortices. *J. Atmos. Sci.* **53**: 3737–3756.
Weckwerth TM. 2000. The effect of small-scale moisture variability on thunderstorm initiation. *Mon. Weather Rev.* **128**: 4017–4030.
Willoughby HE, Jin HL, Lord SJ, Piotrowicz JM. 1984. Hurricane structure and evolution as simulated by an axisymmetric, non-hydrostatic numerical model. *J. Atmos. Sci.* **41**: 1169–1186.
Zhu H, Smith RK. 2002. The importance of three physical processes in a three-dimensional tropical cyclone model. *J. Atmos. Sci.* **59**: 1825–1840.
Zhu H, Smith RK. 2003. Effects of vertical differencing in a minimal hurricane model. *Q. J. R. Meteorol. Soc.* **129**: 1051–1069 (ZS03).
Zhu H, Smith RK, Ulrich W. 2001. A minimal three-dimensional tropical cyclone model. *J. Atmos. Sci.* **58**: 1924–1944 (ZSU).
Zhu H, Smith RK, Ulrich W. 2004. Ocean effects on tropical cyclone intensification and inner-core asymmetries. *J. Atmos. Sci.* **61**: 1245–1258.

DOI: 10.1002/qj